Geosci. Model Dev. Discuss., 7, 9017–9062, 2014
www.geosci-model-dev-discuss.net/7/9017/2014/
doi:10.5194/gmdd-7-9017-2014

Geoscientific Model Development Discussions
Open Access

Modelling the role of fires in the terrestrial carbon balance by incorporating SPITFIRE into the global vegetation model ORCHIDEE – Part 2: Carbon emissions and the role of fires in the global carbon balance

C. Yue[1,2], P. Ciais[2], P. Cadule[2], K. Thonicke[3], and T. T. van Leeuwen[4]

[1]Laboratoire de Glaciologie et Géophysique de l'Environnement, UJF, CNRS, Saint Martin d'Hères, CEDEX, France
[2]Laboratoire des Sciences du Climat et de l'Environnement, LSCE CEA CNRS UVSQ, 91191 Gif-Sur-Yvette, France
[3]Potsdam Institute for Climate Impact Research (PIK) e.V., Telegraphenberg A31, 14473 Potsdam, Germany
[4]Faculty of Earth and Life Sciences, Department of Earth Sciences, VU University Amsterdam, Amsterdam, the Netherlands

Received: 20 November 2014 – Accepted: 1 December 2014 – Published: 18 December 2014

Correspondence to: C. Yue (chao.yue@lsce.ipsl.fr)

Published by Copernicus Publications on behalf of the European Geosciences Union.

GMDD
7, 9017–9062, 2014

Abstract

Carbon dioxide emissions from wild and anthropogenic fires return the carbon absorbed by plants to the atmosphere, and decrease the sequestration of carbon by land ecosystems. Future climate warming will likely increase the frequency of fire-triggering drought; so that the future terrestrial carbon uptake will depend on how fires respond to altered climate variation. In this study, we modelled the role of fires in the global terrestrial carbon balance for 1901–2012, using the global vegetation model ORCHIDEE equipped with the SPITFIRE model. We conducted two simulations with and without the fire module being activated, with a static land cover. The simulated global fire carbon emissions for 1997–2009 are 2.1 $\mathrm{Pg\,C\,yr^{-1}}$, which is close to the 2.0 $\mathrm{Pg\,C\,yr^{-1}}$ as given by the GFED3.1 data. The simulated land carbon uptake after accounting for emissions for 2003–2012 is 3.1 $\mathrm{Pg\,C\,yr^{-1}}$, within the uncertainty of the residual carbon sink estimation (2.8 ± 0.8 $\mathrm{Pg\,C\,yr^{-1}}$). Fires are found to reduce the terrestrial carbon uptake by 0.32 $\mathrm{Pg\,C\,yr^{-1}}$ over 1901–2012, that is 20 % of the total carbon sink in a world without fire. The fire-induced land sink reduction ($\mathrm{SR_{fire}}$) is significantly correlated with climate variability, with larger sink reduction occurring in warm and dry years, in particular during El Niño events. Our results suggest a symmetrical "respiration equivalence" by fires. During the ten lowest $\mathrm{SR_{fire}}$ years ($\mathrm{SR_{fire}}$ = 0.17 $\mathrm{Pg\,C\,yr^{-1}}$), fires mainly compensate the heterotrophic respiration that would happen if no fires had occurred. By contrast, during the ten highest $\mathrm{SR_{fire}}$ fire years ($\mathrm{SR_{fire}}$ = 0.49 $\mathrm{Pg\,C\,yr^{-1}}$), fire emissions exceed their "respiration equivalence" and create a substantial reduction in terrestrial carbon uptake. Our finding has important implication for the future role of fires in the terrestrial carbon balance, because the capacity of terrestrial ecosystems to sequester carbon will be diminished by future climate change characterized by increased drought and more severe El Niño events.

GMDD
7, 9017–9062, 2014

1 Introduction

Vegetation fires contribute significantly to the interannual variability of atmospheric CO_2 concentration. Deforestation and peat fires emit carbon that is not offset by rapid vegetation regrowth, and thus contribute to a net increase of atmospheric CO_2 (Bowman et al., 2009; Langenfelds et al., 2002; Schimel and Baker, 2002; van der Werf et al., 2009). Besides the direct effect of fires in reducing the capacity of terrestrial ecosystems to sequester carbon, other greenhouse gases (e.g., CH_4, N_2O), ozone precursors, and aerosols emitted by fires are a net source of radiative forcing (Podgorny et al., 2003; Tosca et al., 2010; Ward et al., 2012). Finally, fires can also impact climate by changing the land surface properties, such as vegetation structure and albedo (Beck et al., 2011; Jin et al., 2012), as well as the energy partitioning (Liu and Randerson, 2008; Rocha and Shaver, 2011). Changes in temperature and precipitation pattern, in particular drought frequency and severity, also influence fire regimes and their emissions (Balshi et al., 2009; Kloster et al., 2012; Westerling et al., 2011) causing complex fire–vegetation–climate interactions.

The estimation of global carbon emission from fires was pioneered by Seiler and Crutzen (1980), mainly using information from the literature. More recently, large-scale spatially explicit estimation of fire carbon emissions has been aided by satellite-derived burned area and active fire counts (Giglio et al., 2010; Roy et al., 2008; Tansey et al., 2008), as well as vegetation models in which burned area is either prescribed (Randerson et al., 2012; van der Werf et al., 2006, 2010) or simulated with a prognostic fire model (Kloster et al., 2010; Li et al., 2013; Prentice et al., 2011; Thonicke et al., 2010). Several recent estimations have converged to give annual fire carbon emissions of $\sim 2\,\mathrm{Pg\,C\,yr^{-1}}$, as pointed out by Li et al. (2014). Van der Werf et al. (2006) showed that the interannual variability of global fire carbon emissions is decoupled from the variation in burned area, mainly due to the disproportionate contribution to global emissions by fires with a large fuel consumption (forest fire, deforestation fire and peat fire). Prentice et al. (2011) examined how burned area in tropical and subtropical regions is

GMDD
7, 9017–9062, 2014

influenced by the El Niño Southern Oscillation (ENSO) climate variability, and quantified the contribution of fire emission anomaly to the anomaly of land sink as diagnosed by atmospheric inversions. However, it is only recently that Li et al. (2014) have simultaneously constrained the simulated fire carbon emissions and net biome production (NBP, i.e., the land carbon sink) in their absolute terms, from a modelling approach. These modelled components of the carbon balance have rarely been reported simultaneously before. Li et al. (2014) also compared the difference in simulated NBP from two simulations with and without fires. However the specific climatic driving factors for this fire-induced NBP difference have not been investigated. Given the profound perturbation of the climate system by human activities (Cai et al., 2014; Liu et al., 2013; Prudhomme et al., 2013) and with fire activities likely to be increasing in the future (Flannigan et al., 2009; Kloster et al., 2012), it is important to examine how fires and their contribution to global carbon balance have responded to historical climate variations. This knowledge will give us insight into the likely impact of fires on the future land carbon balance.

Just as vegetation can be classified into biomes according to its climatic, morphological and physiological features, so fires occurring under different climate and vegetation patterns have distinctive features that allow them to be characterized by *fire regime*. Attributes of different fire regimes include the frequency, season, size, intensity and extent of fires (Gill and Allan, 2008). Trade-offs may exist between these different aspects of fire, e.g., ecosystems with frequent fires often have a long fire season but can hardly support high-intensity fires because of their low fuel load (Saito et al., 2014). Efforts have been made to further classify fires by examining co-occurring fire characteristics and relating these fire groups (named *pyromes*) to climatic, human and economic factors (Archibald et al., 2013; Chuvieco et al., 2008). Archibald et al. (2013) proposed an approach to divide fires into five pyromes, using the most extensive available global fire regime datasets including fire extent, fire season length, fire return interval, fire size and fire intensity. Though related to the biome distribution, pyromes are different from biomes. For example, the "Intermediate–Cool–Small" fire pyrome occurs throughout

GMDD
7, 9017–9062, 2014

the globe, particular in regions of deforestation and agriculture, whereas the "Frequent–Intense–Large" fire pyrome is associated with tropical grassland-dominated systems. Different fire pyromes are suspected to also have impacts on the amount, seasonality and interannual variability of fire carbon emissions, and further consequences on the terrestrial carbon balance.

In a companion study (Yue et al., 2014), we incorporated the prognostic fire model SPITFIRE into the global vegetation model ORCHIDEE, and evaluated the modelled burned area and fire regimes during the 20th century using multiple observation datasets. In the present study, fire carbon emissions are simulated for 1901–2012, and the role of fires in the terrestrial carbon balance is investigated in relation to different climatic drivers and fire pyromes. In this study, we address the issues of what difference fires have made in the global terrestrial carbon balance, and how this difference is driven by large-scale climate variations, with a special focus on the naturally occurring vegetation fires. More specifically, the objectives of this study are to: (a) Benchmark the ORCHIDEE-SPITFIRE model in terms of simulated carbon emissions against GFED3.1 data, and identify model strengths and weaknesses. (b) Investigate the role of fires in the terrestrial carbon balance for 1901–2012 and the climatic factors driving its magnitude and temporal variation. This objective is tackled by conducting two simulations with and without fire occurrence. (c) Examine the characteristics of different fire regimes (as defined in Archibald et al., 2013) in terms of the role of fires in the terrestrial carbon balance. We hypothesize that more frequent and larger fires will have greater carbon consumption rates than infrequent and smaller ones, and consequently, the fire-induced carbon uptake reduction is larger in the former type of fires.

GMDD
7, 9017–9062, 2014

2 Data and methods

2.1 ORCHIDEE land surface model

ORCHIDEE is a global dynamic vegetation model that simulates the exchange of energy, water and carbon between the atmosphere and the land surface. It is the land surface model of the Earth system model IPSL-CM5 (Dufresne et al., 2013; Krinner et al., 2005). The processes and equations of the SPITFIRE fire model (Thonicke et al., 2010) were implemented in ORCHIDEE, with some modifications being described in Yue et al. (2014). There, the model was evaluated against different satellite observations for simulated burned areas and fire regimes.

The fire combustion completeness (CC) for surface dead fuel was modified. In SPITFIRE, the equations describing surface fuel CC follow Peterson and Ryan (1986), which allow CC to increase with decreasing fuel wetness and level out when it drops below a threshold (see Fig. 1 in Yue et al., 2014). During the model testing, it was found that simulated CC was much higher than the recently compiled field observations for different biomes (van Leeuwen et al., 2014). We thus adjusted the maximum CC for fuel classes of 100 h (with original maximum CC as 1.0) and 1000 h (with original maximum CC as 0.8) to be the same as the mean values given by an earlier version of van Leeuwen et al. (2014) (R. G. Detmers, personal communication, 2013), which was available when preparing the current study. The mean observational values were adopted as the maximum values in the model equations, because the simulated burned area is dominated with low fuel wetness, so that the simulated CC value is close to its maximum. However, we kept the original CC simulation scheme in the original SPITFIRE model for the convenience of future elaboration. According to the earlier version dataset of van Leeuwen et al. (2014) used in this study, the biome-dependent maximum CC is 0.49 for tropical broadleaf evergreen and seasonal dry forests, 0.45 for temperate forests, 0.41 for boreal forests, and 0.85 for grasslands.

The mean CC values for these latter three biomes as updated in van Leeuwen et al. (2014) are 0.69 ± 0.13, 0.47 ± 0.16, and 0.81 ± 0.16 respectively. The CC values

GMDD
7, 9017–9062, 2014

for boreal forests and grasslands used here are within the uncertainty range by van Leeuwen et al. (2014). The CC value for temperate forests is higher than van Leeuwen et al. (2014). Due to the relatively small contribution of temperate forest fires to global fire carbon emissions (4.5 % in our model simulation), we expect the difference in CC values for this biome to have little influence on global emissions. On the other hand, observation-based CC values have a large sampling error and may be revised if more measurements are performed in the future. The implication of the difference in CC values used here and those in van Leeuwen et al. (2014) on estimated fire carbon emissions is briefly discussed in Sect. 3.2.4.

2.2 Model productivity calibration

As shown by Yue et al. (2014), the mean annual burned area for 2001–2006 simulated by ORCHIDEE is 346 Mha yr^{-1}, excluding agricultural fires, which are not represented in the model. This falls within the range 287–384 Mha yr^{-1} from three global satellite-derived datasets (GLOBCARBON, L3JRC and GFED3.1); and is close to the 344 Mha yr^{-1} obtained in GFED3.1 data when agricultural fires are excluded as well. The simulated global burned area during the 20th century was found to agree moderately well with the historical reconstruction by Mouillot and Field (2005), corrected for regional mean bias using GFED3.1 for 1997–2000. One ORCHIDEE model shortcoming is that the terrestrial productivity is generally overestimated (as also revealed by Piao et al., 2013) possibly due to the absence of nutrient limitation, which will lead to overestimation of fire carbon emissions.

The simulated global gross primary productivity (GPP) by ORCHIDEE (version 1.9.6) as driven by CRUNCEP climate forcing data is 205 Pg C yr^{-1} for 1982–2010. This is much higher than the estimated 119 ± 6 Pg C yr^{-1} by Jung et al. (2011), which was derived by interpolating eddy-covariance measurements over the globe using climate and satellite fAPAR and a multiple tree regression ensemble algorithm (hereafter referred to as MTE-GPP). In order to correct for the positive-bias of GPP, we use a simple approach to adjust the optimal carboxylation rates (V_{cmax}, in unit of μmol m^{-2} s^{-1}, see

GMDD
7, 9017–9062, 2014

Eqs. (A2)–(A6) in Krinner et al., 2005) to match the simulated total GPP with the MTE-GPP value reported for different biomes.

The default ORCHIDEE plant functional types (PFTs, excluding bare land) were grouped into five biomes: boreal forest, temperate forest, tropical forest, grassland and agricultural land. The spatial extent of each biome was determined as the area where a corresponding ORCHIDEE PFT occupies more than 90 % of a grid cell in the 0.5° resolution MTE-GPP dataset. A ratio of simulated to MTE-GPP was determined for each biome, and this ratio was used to adjust carboxylation rates (with the maximum potential rate of RuBP regeneration V_{jmax} being set to double the rate V_{cmax}). The original and calibrated carboxylation rates together with the biome-specific GPP ratios are given in Table S1 in the Supplement. We emphasize that the approach employed here is an empirical and simple adjustment to calibrate ORCHIDEE productivity, but does not necessarily result in optimized carboxylation rates that agree with, for example, leaf-scale measurements (e.g., see discussion by Rogers, 2014).

2.3 Simulations and input datasets

To evaluate the role of fires in the global terrestrial carbon balance, two parallel simulations were conducted: fireON and fireOFF, in which SPITFIRE was switched on or off, respectively. In both simulations, the dynamic vegetation module of ORCHIDEE was de-activated, and a current-day vegetation distribution map (converted into the 13-PFT map in ORCHIDEE based on IGBP 1 km vegetation map, http://webmap.ornl.gov/wcsdown/dataset.jsp?ds_id=930) was used as the static land cover. Thus fires associated with land-cover change and resulting carbon emissions were not included in the model.

Agricultural fires were not simulated in the model for two reasons. First, the timing of agricultural burning is strongly constrained by the sowing and harvest date (Magi et al., 2012). An enhanced crop phenology module is under development for ORCHIDEE and this will allow precise agricultural fire seasons to be included in the future. Second, agricultural fires are normally under strict human control and the spread and size

GMDD
7, 9017–9062, 2014

of fires are limited by the size of the fields being burned; they are thus very different from wildfires and warrant a special modelling approach. Carbon emissions from tropical and boreal peat fires are not explicitly simulated, although the model does simulate some burned fraction in tropical regions. Figure S1 in the Supplement compares simulated and GFED3.1 emissions for the tropical region of 20° S–20° N for different types of fire averaged over 1997–2009. The simulated fire emissions were partitioned into forest and grassland fires, and the GFED3.1 emissions were partitioned into "deforestation + forest", "woodland + savanna", and "agriculture + peat". The model could capture part of forest and deforestation fire emissions in this region (simulated 0.28 Pg C yr^{-1} against GFED3.1 0.44 Pg C yr^{-1}). The simulated emissions are slightly lower than GFED3.1 data, even when emissions from agriculture and peat fires are excluded from GFED3.1 (simulated 1.38 Pg C yr^{-1} for forest + grassland; against GFED3.1 1.50 Pg C yr^{-1} for deforestation + forest + woodland + savanna, and 1.63 Pg C yr^{-1} when agriculture and peat are further included). This shows that the model has limited capability in capturing fire emissions in tropical regions.

Both fireON and fireOFF simulations followed the same protocol, which comprised three steps. For both simulations, the model was first run for 200 years (including a 3000 year soil-only spin-up to speed up the equilibrium of slow and passive soil carbon pools) starting from bare ground without fire, with atmospheric CO_2 being fixed at the pre-industrial level (285 ppm) and climate data of 1901–1930 being cycled. For the fireON simulation, after this first spin-up, the model was run for a second spin-up of 150 years with the fire model being switched on, to allow carbon stocks to reach an equilibrium state under pre-industrial fire disturbance. For this second spin-up with fires, atmospheric CO_2 was set at pre-industrial level and climate data of 1901–1930 were cycled. This simulation was followed by a third transient simulation for 1850–2012, with variable climate, atmospheric CO_2 and population density data.

The fireOFF simulation follows the same first spin-up, second spin-up and transient steps as the fireON simulation, except that the fire model is switched off throughout all simulations. The climate data used for 1901–2012 are 6 hourly CRUNCEP data

GMDD
7, 9017–9062, 2014

(http://dods.extra.cea.fr/store/p529viov/cruncep/V4_1901_2012/readme.htm). During the period 1850–1900 when CRUNCEP climate data were not available, the data of 1901–1910 were used and cycled. Lightning data were retrieved from the High Resolution Monthly Climatology of lightning flashes by the Lightning Imaging Sensor–Optical Transient Detector (LIS/OTD) (http://gcmd.nasa.gov/records/GCMD_lohrmc.html). The LIS/OTD dataset provides mean monthly flash rates over the period of 1995–2000 on a 0.5° grid, which were cycled each year throughout the simulation. The annual historical population density data were retrieved from the Netherlands Environmental Assessment Agency (http://themasites.pbl.nl/tridion/en/themasites/hyde/download/index-2.html). Please refer to Yue et al. (2014) for the detailed information on these input datasets.

For the fireON simulation, after the second spin-up, there is a global carbon sink of $0.19\,\mathrm{Pg\,C\,yr^{-1}}$ over the last 50 years prior to the transient simulation due to the not-fully complete equilibrium of slow soil carbon pools. We verified that this sink has a negligible trend (annual trend of $0.003\,\mathrm{Pg\,C\,yr^{-1}}$). For the fireOFF simulation, the residual sink before the transient simulation is $0.17\,\mathrm{Pg\,C\,yr^{-1}}$ (with a negligible annual trend of $-0.001\,\mathrm{Pg\,C\,yr^{-1}}$). Because the ORCHIDEE version used here is very computationally expensive, we did not run the model until a complete carbon saturation state. The simulated annual global total net biome production (NBP) during 1901–2012 was bias-corrected for this incomplete spin-up by subtracting the remaining positive NBP over the last 50 years of the second spin-up. No spatial corrections were made.

2.4 Land–atmosphere carbon flux conventions

We define NEP, the net ecosystem production, as:

$$\mathrm{NEP} = \mathrm{NPP} - \mathrm{RH} - \mathrm{CH} \quad (1)$$

where NPP is net primary production, RH is the heterotrophic respiration, and CH is the harvested crop yield. We assume that crop harvest is released into the atmosphere within the year when being harvested. Because we do not include other components of

GMDD
7, 9017–9062, 2014

the carbon balance term (e.g., wood harvest, herbivore consumption, biogenic volatile organic compound emissions, lateral carbon transfer by rivers and erosion), NEP is considered to be equal to the net terrestrial carbon balance for the fireOFF simulation. Next, we define NBP, the net biome production in the fireON simulation as:

$$NBP = NEP - FE \quad (2)$$

where FE is fire carbon emission. We expect that fires reduce the NBP sink, and define the "fire-induced sink reduction" as:

$$SR_{fire} = NEP_{OFF} - NBP_{ON} \quad (3)$$

where NEP_{OFF} is NEP by fireOFF simulation and NBP_{ON} is NBP by fireON simulation. We further define a term "sink efficiency (SE)" as NBP divided by NPP in the fireON simulation, and NEP divided by NPP in the fireOFF simulation. The sink efficiency describes the fraction of NPP used to sequester carbon from the atmosphere.

2.5 Evaluation datasets and other datasets

The GFED3.1 fire carbon emissions from the CASA biosphere model forced by GFED3.1 burned area data were used to evaluate simulated fire carbon emissions (van der Werf et al., 2010). Much work has been done to calibrate the CASA model against observations, e.g., in terms of productivity and NPP allocation (van der Werf et al., 2006, 2010). Carbon emissions from six different types of fire are identified in GFED3.1 data, namely forest fire, grassland fire, woodland fire, agricultural fire, deforestation and peatland fire. For the convenience of description, emission sources by the former three types of fire are tentatively referred to as natural sources (that ORCHIDEE-SPITFIRE simulates explicitly), and those of the latter three types as anthropogenic sources (that ORCHIDEE does not explicitly include, although it is able to capture part of the deforestation fires as outlined in Sect. 2.3).

Not all anthropogenic carbon emissions (mainly from fossil fuel consumption, cement production and deforestation) into the atmosphere remain there, and parts are

GMDD
7, 9017–9062, 2014

absorbed by the terrestrial ecosystem (land sink) and the ocean (ocean sink). The so-called residual carbon sink in land ecosystems can be obtained by subtracting the annual CO_2 accumulation in the atmosphere and the ocean sink from the total anthropogenic carbon emission (Le Quéré et al., 2013). This residual sink was used here to be compared with simulated carbon sink.

The fire variability at global and regional scales is known to relate to the El Niño Southern Oscillation (ENSO) mode of climate variability (Kitzberger et al., 2001; Prentice et al., 2011; van der Werf et al., 2004), mainly affecting the tropics but with global teleconnections (Kiladis and Diaz, 1989). The Southern Oscillation Index (SOI, http://www.bom.gov.au/climate/current//soihtm1.shtml) is an indicator of the development and intensity of El Niño or La Niña events in the Pacific Ocean (negative values of the SOI below −8 often indicate El Niño episodes and the reverse La Niña episodes). SOI was used here to investigate the fire-induced sink reduction in relation to this large-scale climate oscillation.

Finally, the fire pyrome distribution map of Archibald et al. (2013) was used to relate the influence of fires on NBP to different fire pyromes (Fig. S2). Five fire pyromes were identified by using a Bayesian clustering algorithm with information on key characteristics of fire regimes – size, frequency, intensity, season and extent. The five pyromes are: FIL (Frequent–Intense–Large); FCS (Frequent–Cool–Small); RIL (Rare–Intense–Large) (RIL); RCS (Rare–Cool–Small) and ICS (Intermediate–Cool–Small). Frequent fires (FIL and FCS) are characterized by large annual burned fractions in areas with a relatively long fire season. Australia has large, intense fires (FIL pyrome), whereas in Africa, smaller less intense fires (FCS) dominate. Rare fires (RIL and RCS) are found in areas with a short fire season, dominating in temperate and boreal regions (see Table 1 and Fig. 2 in Archibald et al., 2013, and the descriptions for more information).

GMDD
7, 9017–9062, 2014

3 Results and discussion

3.1 Calibrated productivity and simulated burned area

The calibration of carboxylation rates significantly improved the model-observation agreement in terms of the distribution of GPP as a function of annual precipitation (Fig. 1). The calibrated model is also able to capture the productivity decrease when annual precipitation exceeds 3000 mm (Fig. 1). The simulated global GPP for 1982–2010 is 125 Pg C yr^{-1}, close to the 119 ± 6 Pg C yr^{-1} given by Jung et al. (2011). The simulated global NPP for 2000–2009 is 61 Pg C yr^{-1}, close to the 54 Pg C yr^{-1} estimated by Zhao and Running (2010) using MODIS satellite data and light-use efficiency conversion factors.

The simulated global burned area for 2001–2006 is 239 Mha yr^{-1}, lower than the original 346 Mha yr^{-1} before calibration (Yue et al., 2014). This reduction of simulated burned area mainly occurs in the regions with high fire frequency where GPP was decreased by the calibration (Fig. 2). After the GPP calibration, the burned fraction of grassland and savanna ecosystems in Africa, Australia and South America, became underestimated compared to GFED3.1 (Fig. 2b and d). The reduction of simulated burned fraction is related to the reduced amount of dead fuel on the surface (Fig. S3) in response to the lower GPP; this reduces fire spread rates and fire sizes.

3.2 Temporal and spatial patterns of global fire carbon emission

3.2.1 Comparison of simulated carbon emissions with GFED3.1 at the global scale

The simulated mean annual global fire carbon emissions for 1997–2009 are 2.1 Pg C yr^{-1}, close to the estimate of 2.0 Pg C yr^{-1} by GFED3.1 data, where emissions from both natural and anthropogenic sources are included (Fig. 3), and higher than the 1.5 Pg C yr^{-1} when peat, deforestation and agricultural fires are excluded from

GMDD
7, 9017–9062, 2014

GFED3.1. The model also simulates lower interannual variability of emissions than GFED3.1, giving a coefficient of variation of 0.05, compared to 0.18 for the GFED3.1 data (0.15 when only natural sources are included in GFED3.1).

The interannual variability of fire carbon emissions is known to be partially decoupled from that of burned area (van der Werf et al., 2006), mainly because emission variability is driven by forest fires having higher fuel consumption, whereas burned area variability is driven by savanna fires with relatively large burned fraction but low fuel consumption. At the global scale, the interannual variability of fire carbon emissions is simulated to be closely related to that of burned area (Fig. S4, giving a correlation coefficient of 0.88 over 1997–2009 – all data detrended). In contrast, the correlation coefficient between GFED3.1 natural source emissions and burned area is 0.52 over the same period (0.04 when emissions from both natural and anthropogenic sources are included), i.e., smaller than ORCHIDEE-SPITFIRE. Thus the interannual variability of carbon emissions is more strongly coupled with that of burned area in ORCHIDEE than in GFED3.1.

3.2.2 Comparison of simulated carbon emissions with GFED3.1 for different regions

Annual fire carbon emissions simulated by ORCHIDEE-SPITFIRE are compared with GFED3.1 data for 1997–2009 for different regions in Fig. 4 (see figure caption for expansion of GFED abbreviations and Fig. S5 for a map). The three regions with the most frequent fires, Northern Hemisphere Africa (NHAF), Southern Hemisphere Africa (SHAF) and Australia (AUST) have a total fire emission of 1.17 $\mathrm{Pg\,C\,yr^{-1}}$ and contribute 59 % of the global total emissions in GFED3.1. In ORCHIDEE, annual emissions are 1.18 $\mathrm{Pg\,C\,yr^{-1}}$ for these three regions; an overestimation in NHAF being partly compensated by underestimation in SHAF.

The GFED3.1 data have very small emissions in Temperate North America (TENA), Middle East (MIDE), Central Asia (CEAS) and Europe (EURO) (50 $\mathrm{Tg\,C\,yr^{-1}}$ in total for the three regions; 2.5 % of the global total), whereas ORCHIDEE-SPITFIRE simu-

GMDD
7, 9017–9062, 2014

lates much higher emissions (294 Tg C yr^{-1}; 14 % of the global total) probably because forest fire control measures (Fernandes et al., 2013; Keeley et al., 1999) and forest management in temperate countries (Fang et al., 2001; Luyssaert et al., 2010) are not modelled; this leads to higher burned area and/or higher fuel load in the model. The overestimation of emissions in these three regions is at least partly driven by the overestimation of burned area (annual burned area of 70.2 Mha yr^{-1} in the model vs. 10.1 Mha yr^{-1} in GFED3.1 in Table 1).

The three regions where the model underestimates carbon emissions are Boreal Asia (BOAS), Southeast Asia (SEAS) and Equatorial Asia (EQAS), with simulated emissions of 103 Tg C yr^{-1} (4.9 % of the global total), compared with 412 Tg C yr^{-1} in GFED3.1 (21 % of the global total). The low bias of emissions in BOAS and SEAS is explained by the underestimation of burned area (Table 1) whereas for EQAS, underestimates in both burned area and fuel consumption by the model are found (Table 1) (in particular, peat burning that dominates emissions in 1997–98 in SEAS is lacking in the model, see van der Werf et al., 2008). This points to the need to explicitly include deforestation and peat fires, which are associated with a high amount of fuel consumption (van der Werf et al., 2010).

3.2.3 Fire fuel consumption and latitudinal pattern of emissions

Simulated fuel consumption (g C per m^2 of area burned) in fire is compared to GFED3.1 data in Fig. 5. Both ORCHIDEE-SPITFIRE and GFED3.1 show a large amount of fuel consumption in boreal regions. But fuel consumption in the Russian boreal forest is smaller in the model than GFED3.1 (simulated 400–2000 g C m^{-2} compared to 2000–5000 g C m^{-2} in GFED3.1). The model also fails to capture the high fire fuel consumption (5–20 kg C m^{-2}) at the southern edge of the Amazonian rainforest and in Southeast Asia, which are associated with deforestation fires or peat fires (see also Figs. 6 and 13 in van der Werf et al., 2010). The fire fuel consumptions for savannas and woodland savannas in Africa and Australia are higher in the model than GFED3.1, with

GMDD
7, 9017–9062, 2014

fuel consumption in northern Africa of 1000–2000 g C m^{-2} against 200–1000 g C m^{-2} by GFED3.1. In southern Africa, ORCHIDEE produces fuel consumption of 1000–2000 g C m^{-2} against only 400–1000 g C m^{-2} in GFED3.1.

Figure 6 shows carbon emissions per grid cell area (g C m^{-2} of grid cell) calculated as the product of fire fuel consumption (Fig. 5) and burned fraction (Fig. 2). Because underestimated burned fractions in African and Australian savannas and woodland savannas compensate for overestimated fuel consumption, fire carbon emissions per grid cell for these regions are of similar magnitude to those in GFED3.1. Emissions per grid cell area in southern African woodland savanna are even underestimated by ORCHIDEE (10–50 g C m^{-2} yr^{-1}) compared with GFED3.1 (50–200 g C m^{-2} yr^{-1}), due to the great underestimation in burned area.

By looking at the latitudinal distribution of burned area and emission, the systematic error in ORCHIDEE's estimated emissions can be clearly related to that in burned area (Fig. 7). The underestimation of burned area in tropical and subtropical regions (30° S–15° N) (Fig. 2) is compensated by the overestimated fire fuel consumption. In southern tropical regions (0–30° S), carbon emissions are still underestimated (by 270 Tg C yr^{-1}) despite this compensation effect, whereas in northern tropical regions (0–15° N), the compensation leads to overestimated emissions (by 190 Tg C yr^{-1}) compared with GFED3.1.

3.2.4 Attributing systematic emission errors to burned area and fuel consumption at regional level

Table 1 compares mean annual simulated and GFED3.1 emissions for 1997–2009 for different regions. The model bias of emissions is qualitatively attributed to those of burned area and fuel consumption. Table S2 further compares NPP and fire combustion completeness between the model and the GFED3.1 data (where NPP is from the CASA biosphere model, with all GFED3.1 data in Table S2 obtained from Table 4 in van der Werf et al., 2010). For all regions (except NHAF and AUST) where emissions are

GMDD
7, 9017–9062, 2014

overestimated by the model (TENA, CEAM, NHSA, SHSA, EURO, MIDE, CEAS), there is a coincident overestimation in burned area, which sometimes overrides the underestimated fuel consumption in regions such as CEAM. Regions where emissions are underestimated also show underestimated burned area (with the exception of BOAS), some of them also having underestimated fuel consumption (EQAS).

The simulated NPP regional averages are in general agreement with those from the CASA model reported by van der Werf et al. (2010) (Table S2), indicating that the simulated fuel load might be comparable to GFED3.1 data, and that systematic errors in fuel consumption might be dominated by errors in the combustion completeness of different fuels. On the one hand, simulated combustion completeness for litter agrees well with the values used in GFED3.1; but on the other hand, combustion completeness for the litter and aboveground live biomass combined is much higher in ORCHIDEE than GFED3.1 over BOAS, BONA, MIDE, NHAF, SHAF and AUST, and much lower over EQAS. This might reflect a higher or lower simulated combustion completeness of tree live biomass, which needs further investigation. The higher simulated combustion completeness for litter and live biomass combined in NHAF, SHAF and AUST explains the higher fuel consumptions in these regions, given the fact that simulated NPP is rather similar to GFED3.1 over these regions (except for NHAF where the simulated NPP is 40 % higher than GFED3.1 and combustion completeness is 2.6 times higher). One should also keep in mind that GFED3.1 is not a solely observational dataset, but is another model calculation of fire emissions and their component drivers. Given the availability of the comprehensive fuel combustion field data recently compiled by van Leeuwen et al. (2014), more careful calibration and validation of the simulated combustion completeness for different fuel types could be performed in the future.

Finally, the combustion completeness (CC) values used for the 100 and 1000 h dead fuel in the model for temperate forests, boreal forests and grasslands are slightly different from those reported by van Leeuwen et al. (2014), as described at the end of Sect. 2.1. We tried a simple approach to adjust the simulated fire carbon emissions for these three biomes by multiplying the simulated emissions by the ratio of our CC

GMDD
7, 9017–9062, 2014

values to those of van Leeuwen et al. (2014), and found that the global total fire carbon emission remains almost the same (2.1 Pg C yr^{-1} vs. 2.08 Pg C yr^{-1} before and after adjustment for 1997–2009). This is because the smaller CC values used for temperate and boreal forests are compensated for by the larger CC value of grasslands used in the model.

3.3 The role of fires in the terrestrial carbon balance

3.3.1 The simulated carbon balance for the last decade (1993–2012)

Figure 8 shows the percentage of NPP emitted by fire over the last decade (2003–2012). Regions with frequent burning show a higher fraction of NPP being returned to the atmosphere by fire. Yet, heterotrophic respiration remains the dominant pathway for returning NPP to the atmosphere, accounting for 85.7 % of the global NPP (91.0 % when agricultural harvest is included, the CH term in Eq. 1). Fire carbon emissions account for 3.4 % of NPP, with the remaining 5.2 % of NPP being accumulated in the biosphere as a carbon sink (NBP). The simulated global NPP for 2003–2012 is 60 Pg C yr^{-1} in the fireON simulation, with 2.1 Pg C yr^{-1} emitted as fire emissions, and 3.1 Pg C yr^{-1} stored as NBP. The simulated NBP is within the 1-sigma error of the observed residual sink for the same period, which is of 2.8 ± 0.8 Pg C yr^{-1} (see Le Quéré et al., 2013 for uncertainty estimation).

3.3.2 Fire-induced terrestrial carbon sink reduction for 1901–2012

The different components of global carbon fluxes for the fireON and fireOFF simulations are shown in Fig. 9. Net primary production (NPP) for fireON and fireOFF are very similar (NPP is 6 Tg C yr^{-1} higher in fireOFF for 1901–2012) (Fig. 9a). This greater NPP in the fireOFF simulation compared with fireON might be underestimated, because land-cover change or vegetation dynamics were ignored in the simulations (For

GMDD
7, 9017–9062, 2014

example, bigger forest coverage would occur in fireOFF if vegetation dynamics were modelled).

The carbon sink in fireOFF (NEP_{OFF}) is greater than that in fireON (NBP_{ON}) (Fig. 9c). This is because fire emissions (1.91 Pg C yr^{-1} for 1901–2012) are greater than the heterotrophic respiration excess in fireOFF (Fig. 9b, by 1.62 Pg C yr^{-1} averaged over 1901–2012). NEP in fireOFF minus NBP in fireON is the fire-induced sink reduction (SR_{fire}), amounting to 0.32 ± 0.09 Pg C yr^{-1} over 1901–2012, or 20 % of the fireOFF NEP. This sink reduction would have been bigger if deforestation (land-cover change) and peat fires had been included in the model because carbon released from these fires is more likely an irreversible net carbon source, i.e., it will not be re-absorbed by post-fire plant recovery on a centennial time scale.

The small fire-induced carbon sink reduction obtained in this study, when only natural wildfires are modelled and with static vegetation cover, implies that if carbon stocks in the fuel (dominated by litter or organic soil except in the cases of peat or deforestation fires) were not consumed in fires, they would have been decomposed and have contributed to the heterotrophic respiration. This suggests a "fire respiration equivalence" in the model. I.e., fire carbon emissions are somewhat analogous to heterotrophic respiration, and only when fires are extreme do their emissions exceed the role of respiration, causing a net reduction in carbon sink in FireON compared to FireOFF. The sink reduction variability is closely correlated with fire emission anomalies during 1901–2012 (with a correlation coefficient of 0.71, Fig. 9d). Fire carbon emissions show an acceleration of 1.8 Tg C yr^{-2} prior to 1970, and a trend of 6 Tg C yr^{-2} after 1970, with both trends being significant at the 0.05 level.

Our simulated cumulative land carbon storage (NBP) for 1959–2012 is 109.6 Pg C (with 80.8 Pg C stored in live biomass and 28.8 Pg C in litter and soil), which is close to the cumulative residual sink of 105.9 Pg C (Le Quéré et al., 2013). The cumulative land sink in fireOFF is 127.2 Pg C, suggesting a cumulative sink reduction of 17.6 Pg C by fire since 1959. The correlation coefficient between detrended time series of NBP by the fireON simulation and the residual sink is 0.59, indicating that the model is moderately

GMDD
7, 9017–9062, 2014

successful at capturing the interannual variability of the carbon sink by the terrestrial ecosystem.

Prentice et al. (2011) pointed out that fire emissions account for one-third and one-fifth of the interannual variation of the 1997–2005 global carbon balance as indicated by atmospheric inversions, when emissions were from the GFED3.1 data and simulated by the vegetation model LPX, respectively. In our study, fire carbon emissions explained 20 % of the interannual variation of simulated NBP (which is the R^2 of the linear regression of detrended annual NBP against simulated carbon emission), similar to their result.

3.3.3 Fire-induced carbon sink reduction for extreme high and low fire years

We selected ten "high fire years" years as the ten years with highest fire-induced sink reduction (SR_{fire}) during 1901–2012 (Fig. 9d), and ten "low fire years" as the years with the ten lowest SR_{fire} during the same period. The ten high fire years are: 1913, 1970, 1979, 1983, 1994, 1995, 1998, 2000, 2002 and 2012. Nine out of ten years occur after 1970 – congruent with the significant global temperature increase after 1970 (Hartmann et al., 2013). The SR_{fire} for the high fire years is 0.49 Pg C yr^{-1} (23 % of the fireOFF NEP), compared with an SR_{fire} of 0.17 Pg C yr^{-1} (7 % of the fireOFF NEP) for the ten low fire years.

The Pearson correlation coefficient (r) between the SR_{fire} time series and other model variable or climatic drivers (temperature, precipitation) was used to investigate the driving factors for fire-induced sink reduction. The SR_{fire} variation was found to be best explained by fire numbers ($r = 0.65$, $p < 0.05$) within the model, since fire numbers are also driving the variation of burned area ($r = 0.81$, $p < 0.05$). SR_{fire} is also positively correlated with land surface temperature ($r = 0.16$, $p = 0.08$), and negatively correlated with precipitation ($r = -0.23$, $p < 0.05$), although the correlation is fairly weak.

The opposite of SR_{fire} is positively correlated with the Southern Oscillation Index (SOI) ($r = 0.29$, $p < 0.05$, Fig. 10), suggesting that global fire-induced sink reduction is significantly related to the change in the tropical Pacific sea-surface temperature gradi-

GMDD
7, 9017–9062, 2014

ent, because of its strong influence over global rainfall (Ropelewski and Halpert, 1987, 1996). The El Niño state (i.e., low SOI value) of climate oscillation generally coincides with larger sink reduction by fires (i.e., larger SR_{fire}), and La Niña with smaller reduction. Indeed, seven out of the ten high fire years occur during El Niño episodes, and six out of the ten low fire years occur during La Niña episodes (The diagnosis of El Niño and La Niña episodes are given by the Bureau of Meteorology of Australian government, http://www.bom.gov.au/climate/enso/lnlist/). SR_{fire} is more strongly related with SOI in tropical regions than at the global scale thanks to the more direct impacts of ENSO events (for 30° S–30° N, the relationship between $-SR_{fire}$ and SOI yields $r = 0.33$ with $p < 0.05$). This region contributes 82 and 72 % of global total emissions and carbon sink, respectively.

As we did not include agricultural fires, deforestation fires and peat fires in our simulation, the analysis of fire-induced sink reduction related to climate variations presented here mainly represents a scenario of naturally occurring fires. Given that these anthropogenic fires are closely dependent on climate conditions (e.g., as shown by van der Werf et al., 2004, 2008), the actual correlation between fire-induced sink reduction and SOI over the historical period might be underestimated by the model.

Nevertheless, the suggested "respiration equivalence" of fires (i.e., larger sink reduction with more extreme fires), and the strong relevance of SR_{fire} to climatic variations (i.e., larger sink reduction during warm and dry El Niño years) have implications for the future role of fires in the terrestrial carbon balance. Studies show that climate warming in recent decades has already driven boreal fire frequency to exceed its historical limit (Kelly et al., 2013) and resulted in accelerated carbon loss (Hayes et al., 2011; Mack et al., 2011; Turetsky et al., 2011). The ENSO-driven climate variability, with its strong influence on global precipitation, has widespread impact on fire activity across the globe (Carmona-Moreno et al., 2005; Kitzberger et al., 2001; Chen et al., 2011; Prentice et al., 2011). With continuing anthropogenic disturbances on the climate system by greenhouse gas emissions, the evidence from multiple-modelling exercises indicates a likely increase in the frequency of El Niño events and extreme drought in the

GMDD
7, 9017–9062, 2014

21st century (Cai et al., 2014; Meehl and Washington, 1996; Prudhomme et al., 2013; Timmermann et al., 1999). These projections in turn lead to projected increases in fire activities and emissions (Flannigan et al., 2009; Kloster et al., 2012). As a further consequence, the capacity for land ecosystems to sequester carbon is likely to be further diminished in the future.

3.3.4 Simulated fire-induced sink reduction and comparison with Li et al. (2014)

Li et al. (2014) investigated the role of fires in the terrestrial carbon cycle using the CLM4.5 model and a similar modelling approach (fire-on vs. fire-off simulations, with prescribed historical land cover and a de-activated dynamic vegetation module). They found that fires reduced the terrestrial carbon sink by on average 1.0 $\mathrm{Pg\,C\,yr^{-1}}$ during the 20th century. Our simulated sink reduction (0.32 $\mathrm{Pg\,C\,yr^{-1}}$ for 1901–2012) is smaller than theirs. However, fire carbon emissions (called the *fire direct effect* by Li et al., 2014) by the two studies are similar (1.9 $\mathrm{Pg\,C\,yr^{-1}}$ by both studies for the 20th century). Therefore, the difference in fire sink reduction between the two studies must be due to differences in other flux estimates (NPP and heterotrophic respiration).

Li et al. (2014) estimated that fire reduced global NPP by 1.9 $\mathrm{Pg\,C\,yr^{-1}}$, but the heterotrophic respiration was reduced by an even larger amount (2.7 $\mathrm{Pg\,C\,yr^{-1}}$), resulting in a higher NEP of 0.9 $\mathrm{Pg\,C\,yr^{-1}}$ in their fire-off simulation (called *fire indirect effect*). We also find a higher heterotrophic respiration in our fireOFF simulation (by on average 1.62 $\mathrm{Pg\,C\,yr^{-1}}$ over 1901–2012) but the simulated NPP difference is negligible (6 $\mathrm{Tg\,C\,yr^{-1}}$ higher in fireOFF than fireON). The NPP reduction by fire is probably underestimated in our study, because land-cover change fires are not accounted for, and grassland or agricultural land converted from forest has much lower NPP than it had prior to conversion (Houghton et al., 1999). Thus the NEP increase by switching fire off might also be underestimated, which leads to underestimated sink reduction by fire.

Lastly, our study shares two prominent uncertainties in quantifying the role of fires in the terrestrial carbon cycle with those discussed by Li et al. (2014). Firstly, the vegetation dynamics module was switched off in our simulation, and this might limit the

GMDD
7, 9017–9062, 2014

terrestrial carbon sink by land ecosystems in a world without fire. Previous studies have pointed out that if all fires were suppressed tree cover would expand in regions where current grassland or woodland ecosystems are maintained by fires (Bond et al., 2005; Staver et al., 2011); and that the expanded forest coverage would increase land carbon stock (Bond et al., 2005). Secondly, because ORCHIDEE was not coupled to an atmosphere model, the atmospheric concentration changes for various gases released by fire, or a complete fire–vegetation–climate feedback, as discussed in the Introduction, were not included.

3.3.5 The role of fires in the terrestrial carbon balance in relation to fire pyromes

We compared fire fuel consumption, the fraction of NPP returned via fire emissions and its temporal variation, and carbon sink efficiencies (SE) for fireOFF and fireON simulations for the five pyromes defined by Archibald et al. (2013) (see Sect. 2.5). The temporal variation for the fraction of NPP by fire emissions is examined as the coefficient of variation during 1901–2012, which is the standard deviation divided by the mean.

According to model simulation, Frequent–Intense–Large (FIL) and Frequent–Cool–Small (FCS) fires have higher fuel consumption than infrequent Rare–Intense–Large (RIL) and Rare–Cool–Small (RCS) fires (Fig. 11), fuel consumption being the highest in the FCS pyrome ($1.2\,\mathrm{kg\,C\,m^{-2}}$) and the lowest in the RCS pyrome ($0.6\,\mathrm{kg\,C\,m^{-2}}$). Correspondingly, the ratio of fire emission to NPP is also higher in frequent-fire pyromes than in infrequent ones, but the temporal variation of this fraction is higher for RCS and RIL pyromes. Regions with infrequent fires (RCS, RIL and ICS) have greater sink efficiency than those with frequent ones (FIL, FCS) for the fireOFF simulation. This pattern remains for the fireON simulation, which gives smaller sink efficiency than fireOFF for all the pyromes, due to the adverse effects of fires on the land carbon sink. Consequently, the sink efficiency as reduced by fires remains higher in infrequent-fire pyromes (being the highest in the RIL pyrome) than frequent ones (being the lowest in the FIL pyrome).

GMDD
7, 9017–9062, 2014

It is reasonable to find that frequent fires have higher fuel consumption than small cool ICS and RCS fires, because the latter are generally human-controlled burning with limited fuel load (Archibald et al., 2013). However, intuitively, the Rare–Intense–Large (RIL) fires are expected to have at least comparable, if not larger, fuel consumption than the FIL and FCS pyromes, since their spatial extent covers the North American boreal forest biome where large amounts of soil (and biomass) carbon stocks are exposed to burning. Our model simulation does show a high amount of fire fuel consumption in North American boreal forests: 1–5 $kg\,C\,m^{-2}$ (Fig. 5), comparable to that reported in regional studies (French et al., 2011; Kasischke and Hoy, 2012). A closer examination of the fire pryome distribution map (Fig. S2) reveals that some of the grassland fires in central and eastern Asia and inland Australia are also classified as RIL fires, which have a rather low simulated fuel consumption rate (1–200 $g\,C\,m^{-2}$, Fig. 5). Thus the simulated fuel consumption for RIL fires is a mean value for all above regions (including boreal forests in Eurasia as well), which is lower than frequent fires.

We also find the carbon sink efficiencies for infrequent-fire pyromes are higher than frequent ones for both fireON and fireOFF simulations, probably because more forests are located in infrequent-fire pyromes (Table 1, Archibald et al., 2013). The sink efficiency reduction (SE_{OFF}–SE_{ON}) by fires is the highest in the RIL pyrome, congruent with a higher Emission-to-NPP fraction. If we examine the percentage of fire-induced sink efficiency reduction to SE_{OFF}, the FIL, FCS and RIL pyromes emerge again to have higher percentage than RCS and ICS pyromes (data not shown). This indicates that frequent fires and infrequent-large fires reduce the carbon sequestration capacity of land ecosystems to a higher extent. Note that as an initial attempt to understand the role of fires in carbon cycling for different pyromes (such as that for different biomes), great uncertainties exist in the modelling results presented here. Sources of uncertainties include that agricultural and deforestation fires were included in Archibald et al. (2013) but not in our model; errors and uncertainties exist in simulated fire fuel consumption and fire emissions; the combustion difference between surface fires in boreal Eurasian

GMDD
7, 9017–9062, 2014

forests and crown fires in North American boreal forests (de Groot et al., 2013; Wirth, 2005) is lacking in the model; uncertainties exist in the classification of fire pyromes.

4 Summary and conclusions

In this study, we modelled fire emissions and the role of fires in the terrestrial carbon balance for the 20th century, using the ORCHIDEE land surface model with recently integrated SPITFIRE model and with a static land cover. The simulated global fire carbon emissions for 1997–2009 are 2.1 $\mathrm{Pg\,C\,yr^{-1}}$, which is close to the 2.0 $\mathrm{Pg\,C\,yr^{-1}}$ given by the GFED3.1 data (when all types of fires are included), owing to error compensation among different regions in the model. Fire carbon emissions are mainly underestimated in Southern Hemisphere tropical regions and this error is compensated by an overestimation in temperate ecosystems. The regional emission errors are found to be coincident with the errors in simulated burned area, with the exception that fire fuel consumption is underestimated in regions featuring peatland or deforestation fires such as equatorial Asia, because these fires are not explicitly included in the model.

Fires reduced the terrestrial carbon uptake by on average 0.32 $\mathrm{Pg\,C\,yr^{-1}}$ over the period 1901–2012, equivalent to 20 % of the carbon sink in a world without fire. Our simulation results suggest that fires have a "respiration equivalence" (although the inclusion of dynamic vegetation in the model might change this). Fire emissions in low fire years mainly compensate for heterotrophic respiration that would occur without fire combustion, but emissions in extreme high fire years exceed the "respiration equivalence" and create a substantial reduction in the terrestrial carbon sink. This fire-induced sink reduction has been found to be significantly correlated with climatic variations including El Niño Southern Oscillation (ENSO), with larger sink reductions occurring in warm, dry El Niño episodes. This finding has an important implication for the future role of fires in the terrestrial carbon balance, because the capacity of terrestrial ecosystems to sequester carbon will be more likely diminished in a future climate with more frequent and intense droughts and more extreme El Niño events. This also implies that fires may

GMDD
7, 9017–9062, 2014

significantly impact the climate-carbon response (known as the γ factor) as simulated by coupled climate-carbon models.

The Supplement related to this article is available online at doi:10.5194/gmdd-7-9017-2014-supplement.

Acknowledgements. We thank S. Archibald for providing the fire pyrome distribution map. Funding for this work was provided by the ESA firecci project (http://www.esa-fire-cci.org/) and EU FP7 project PAGE21.

References

Archibald, S., Lehmann, C. E. R., GómezsDans, J. L., and Bradstock, R. A.: Defining pyromes and global syndromes of fire regimes, P. Natl. Acad. Sci. USA, 110, 6442–6447, doi:10.1073/pnas.1211466110, 2013.

Balshi, M. S., McGuire, A. D., Duffy, P., Flannigan, M., Kicklighter, D. W., and Melillo, J.: Vulnerability of carbon storage in North American boreal forests to wildfires during the 21st century, Glob. Change Biol., 15, 1491–1510, 2009.

Beck, P. S. A., Goetz, S. J., Mack, M. C., Alexander, H. D., Jin, Y., Randerson, J. T., and Loranty, M. M.: The impacts and implications of an intensifying fire regime on Alaskan boreal forest composition and albedo, Glob. Change Biol., 17, 2853–2866, doi:10.1111/j.1365-2486.2011.02412.x, 2011.

Bond, W. J., Woodward, F. I., and Midgley, G. F.: The global distribution of ecosystems in a world without fire, New Phytol., 165, 525–537, doi:10.1111/j.1469-8137.2004.01252.x, 2005.

Bowman, D. M. J. S., Balch, J. K., Artaxo, P., Bond, W. J., Carlson, J. M., Cochrane, M. A., D'Antonio, C. M., DeFries, R. S., Doyle, J. C., Harrison, S. P., Johnston, F. H., Keeley, J. E., Krawchuk, M. A., Kull, C. A., Marston, J. B., Moritz, M. A., Prentice, I. C., Roos, C. I., Scott, A. C., Swetnam, T. W., van der Werf, G. R., and Pyne, S. J.: Fire in the Earth system, Science, 324, 481–484, doi:10.1126/science.1163886, 2009.

Cai, W., Borlace, S., Lengaigne, M., van Rensch, P., Collins, M., Vecchi, G., Timmermann, A., Santoso, A., McPhaden, M. J., Wu, L., England, M. H., Wang, G., Guilyardi, E., and Jin, F.-F.:

GMDD
7, 9017–9062, 2014

Increasing frequency of extreme El Nino events due to greenhouse warming, Nature Clim. Change, 4, 111–116, doi:10.1038/nclimate2100, 2014.
Carmona-Moreno, C., Belward, A., Malingreau, J.-P., Hartley, A., Garcia-Alegre, M., Antonovskiy, M., Buchshtaber, V., and Pivovarov, V.: Characterizing interannual variations in global fire calendar using data from Earth observing satellites, Glob. Change Biol., 11, 1537–1555, doi:10.1111/j.1365-2486.2005.01003.x, 2005.
Chen, Y., Randerson, J. T., Morton, D. C., DeFries, R. S., Collatz, G. J., Kasibhatla, P. S., Giglio, L., Jin, Y., and Marlier, M. E.: Forecasting fire season severity in South America using sea surface temperature anomalies, Science, 334, 787–791, doi:10.1126/science.1209472, 2011.
Chuvieco, E., Giglio, L., and Justice, C.: Global characterization of fire activity: toward defining fire regimes from Earth observation data, Glob. Change Biol., 14, 1488–1502, 2008.
De Groot, W. J., Cantin, A. S., Flannigan, M. D., Soja, A. J., Gowman, L. M., and Newbery, A.: A comparison of Canadian and Russian boreal forest fire regimes, Forest Ecol. Manag., 294, 23–34, doi:10.1016/j.foreco.2012.07.033, 2013.
Dufresne, J.-L., Foujols, M.-A., Denvil, S., Caubel, A., Marti, O., Aumont, O., Balkanski, Y., Bekki, S., Bellenger, H., Benshila, R., Bony, S., Bopp, L., Braconnot, P., Brockmann, P., Cadule, P., Cheruy, F., Codron, F., Cozic, A., Cugnet, D., Noblet, N. de, Duvel, J.-P., Ethé, C., Fairhead, L., Fichefet, T., Flavoni, S., Friedlingstein, P., Grandpeix, J.-Y., Guez, L., Guilyardi, E., Hauglustaine, D., Hourdin, F., Idelkadi, A., Ghattas, J., Joussaume, S., Kageyama, M., Krinner, G., Labetoulle, S., Lahellec, A., Lefebvre, M.-P., Lefevre, F., Levy, C., Li, Z. X., Lloyd, J., Lott, F., Madec, G., Mancip, M., Marchand, M., Masson, S., Meurdesoif, Y., Mignot, J., Musat, I., Parouty, S., Polcher, J., Rio, C., Schulz, M., Swingedouw, D., Szopa, S., Talandier, C., Terray, P., Viovy, N., and Vuichard, N.: Climate change projections using the IPSL-CM5 Earth System Model: from CMIP3 to CMIP5, Clim. Dynam., 40, 2123–2165, doi:10.1007/s00382-012-1636-1, 2013.
Fang, J., Chen, A., Peng, C., Zhao, S., and Ci, L.: Changes in forest biomass carbon storage in China between 1949 and 1998, Science, 292, 2320–2322, doi:10.1126/science.1058629, 2001.
Fernandes, P. M., Davies, G. M., Ascoli, D., Fernández, C., Moreira, F., Rigolot, E., Stoof, C. R., Vega, J. A., and Molina, D.: Prescribed burning in southern Europe: developing fire management in a dynamic landscape, Front. Ecol. Environ., 11, e4–e14, doi:10.1890/120298, 2013.

GMDD
7, 9017–9062, 2014

Flannigan, M. D., Krawchuk, M. A., de Groot, W. J., Wotton, B. M., and Gowman, L. M.: Implications of changing climate for global wildland fire, Int. J. Wildland Fire, 18, 483–507, 2009.
French, N. H. F., de Groot, W. J., Jenkins, L. K., Rogers, B. M., Alvarado, E., Amiro, B., de Jong, B., Goetz, S., Hoy, E., Hyer, E., Keane, R., Law, B. E., McKenzie, D., McNulty, S. G., Ottmar, R., Pérez-Salicrup, D. R., Randerson, J., Robertson, K. M., and Turetsky, M.: Model comparisons for estimating carbon emissions from North American wildland fire, J. Geophys. Res.-Biogeo., 116, G00K05, doi:10.1029/2010JG001469, 2011.
Giglio, L., Randerson, J. T., van der Werf, G. R., Kasibhatla, P. S., Collatz, G. J., Morton, D. C., and DeFries, R. S.: Assessing variability and long-term trends in burned area by merging multiple satellite fire products, Biogeosciences, 7, 1171–1186, doi:10.5194/bg-7-1171-2010, 2010.
Gill, A. M. and Allan, G.: Large fires, fire effects and the fire-regime concept, Int. J. Wildland Fire, 17, 688–695, 2008.
Hayes, D. J., McGuire, A. D., Kicklighter, D. W., Gurney, K. R., Burnside, T. J., and Melillo, J. M.: Is the northern high-latitude land-based CO_2 sink weakening?, Global Biogeochem. Cy., 25, GB3018, doi:10.1029/2010GB003813, 2011.
Houghton, R. A., Hackler, J. L., and Lawrence, K. T.: The U.S. carbon budget: contributions from land-use change, Science, 285, 574–578, doi:10.1126/science.285.5427.574, 1999.
Jin, Y., Randerson, J. T., Goetz, S. J., Beck, P. S. A., Loranty, M. M., and Goulden, M. L.: The influence of burn severity on postfire vegetation recovery and albedo change during early succession in North American boreal forests, J. Geohys. Res.-Biogeo., 117, G01036, doi:10.1029/2011JG001886, 2012.
Jung, M., Reichstein, M., Margolis, H. A., Cescatti, A., Richardson, A. D., Arain, M. A., Arneth, A., Bernhofer, C., Bonal, D., Chen, J., Gianelle, D., Gobron, N., Kiely, G., Kutsch, W., Lasslop, G., Law, B. E., Lindroth, A., Merbold, L., Montagnani, L., Moors, E. J., Papale, D., Sottocornola, M., Vaccari, F., and Williams, C.: Global patterns of land–atmosphere fluxes of carbon dioxide, latent heat, and sensible heat derived from eddy covariance, satellite, and meteorological observations, J. Geohys. Res.-Biogeo., 116, G00J07, doi:10.1029/2010JG001566, 2011.
Kasischke, E. S. and Hoy, E. E.: Controls on carbon consumption during Alaskan wildland fires, Glob. Change Biol., 18, 685–699, doi:10.1111/j.1365-2486.2011.02573.x, 2012.

GMDD
7, 9017–9062, 2014

Keeley, J. E., Fotheringham, C. J., and Morais, M.: Reexamining fire suppression impacts on brushland fire regimes, Science, 284, 1829–1832, doi:10.1126/science.284.5421.1829, 1999.

Kelly, R., Chipman, M. L., Higuera, P. E., Stefanova, I., Brubaker, L. B., and Hu, F. S.: Recent burning of boreal forests exceeds fire regime limits of the past 10,000 years, P. Natl. Acad. Sci. USA, 110, 13055–13060, doi:10.1073/pnas.1305069110, 2013.

Kiladis, G. N. and Diaz, H. F.: Global climatic anomalies associated with extremes in the Southern Oscillation, J. Climate, 2, 1069–1090, doi:10.1175/1520-0442(1989)002<1069:GCAAWE>2.0.CO;2, 1989.

Kitzberger, T., Swetnam, T. W., and Veblen, T. T.: Inter-hemispheric synchrony of forest fires and the El Niño–Southern Oscillation, Global Ecol. Biogeogr., 10, 315–326, doi:10.1046/j.1466-822X.2001.00234.x, 2001.

Kloster, S., Mahowald, N. M., Randerson, J. T., Thornton, P. E., Hoffman, F. M., Levis, S., Lawrence, P. J., Feddema, J. J., Oleson, K. W., and Lawrence, D. M.: Fire dynamics during the 20th century simulated by the Community Land Model, Biogeosciences, 7, 1877–1902, doi:10.5194/bg-7-1877-2010, 2010.

Kloster, S., Mahowald, N. M., Randerson, J. T., and Lawrence, P. J.: The impacts of climate, land use, and demography on fires during the 21st century simulated by CLM-CN, Biogeosciences, 9, 509–525, doi:10.5194/bg-9-509-2012, 2012.

Krinner, G., Viovy, N., de Noblet-Ducoudré, N., Ogée, J., Polcher, J., Friedlingstein, P., Ciais, P., Sitch, S., and Prentice, I. C.: A dynamic global vegetation model for studies of the coupled atmosphere–biosphere system, Global Biogeochem. Cy., 19, GB1015, doi:10.1029/2003GB002199, 2005.

Langenfelds, R. L., Francey, R. J., Pak, B. C., Steele, L. P., Lloyd, J., Trudinger, C. M., and Allison, C. E.: Interannual growth rate variations of atmospheric CO_2 and its $\delta^{13}C$, H_2, CH_4, and CO between 1992 and 1999 linked to biomass burning, Global Biogeochem. Cy., 16, 21-1–21-22, doi:10.1029/2001GB001466, 2002.

Le Quéré, C., Andres, R. J., Boden, T., Conway, T., Houghton, R. A., House, J. I., Marland, G., Peters, G. P., van der Werf, G. R., Ahlström, A., Andrew, R. M., Bopp, L., Canadell, J. G., Ciais, P., Doney, S. C., Enright, C., Friedlingstein, P., Huntingford, C., Jain, A. K., Jourdain, C., Kato, E., Keeling, R. F., Klein Goldewijk, K., Levis, S., Levy, P., Lomas, M., Poulter, B., Raupach, M. R., Schwinger, J., Sitch, S., Stocker, B. D., Viovy, N., Zaehle, S., and Zeng, N.: The

GMDD
7, 9017–9062, 2014

global carbon budget 1959–2011, Earth Syst. Sci. Data, 5, 165–185, doi:10.5194/essd-5-165-2013, 2013.
Li, F., Levis, S., and Ward, D. S.: Quantifying the role of fire in the Earth system – Part 1: Improved global fire modeling in the Community Earth System Model (CESM1), Biogeosciences, 10, 2293–2314, doi:10.5194/bg-10-2293-2013, 2013.
Li, F., Bond-Lamberty, B., and Levis, S.: Quantifying the role of fire in the Earth system – Part 2: Impact on the net carbon balance of global terrestrial ecosystems for the 20th century, Biogeosciences, 11, 1345–1360, doi:10.5194/bg-11-1345-2014, 2014.
Liu, H. and Randerson, J. T.: Interannual variability of surface energy exchange depends on stand age in a boreal forest fire chronosequence, J. Geophys. Res., 113, G01006, doi:10.1029/2007JG000483, 2008.
Liu, J., Wang, B., Cane, M. A., Yim, S.-Y., and Lee, J.-Y.: Divergent global precipitation changes induced by natural versus anthropogenic forcing, Nature, 493, 656–659, doi:10.1038/nature11784, 2013.
Luyssaert, S., Ciais, P., Piao, S. L., Schulze, E.-D., Jung, M., Zaehle, S., Schelhaas, M. J., Reichstein, M., Churkina, G., Papale, D., Abril, G., Beer, C., Grace, J., Loustau, D., Matteucci, G., Magnani, F., Nabuurs, G. J., Verbeeck, H., Sulkava, M., van der Werf, G. R., Janssens, I. A., and Team members of the C.-I. S.: The European carbon balance. Part 3: forests, Glob. Change Biol., 16, 1429–1450, doi:10.1111/j.1365-2486.2009.02056.x, 2010.
Mack, M. C., Bret-Harte, M. S., Hollingsworth, T. N., Jandt, R. R., Schuur, E. A. G., Shaver, G. R., and Verbyla, D. L.: Carbon loss from an unprecedented Arctic tundra wildfire, Nature, 475, 489–492, doi:10.1038/nature10283, 2011.
Magi, B. I., Rabin, S., Shevliakova, E., and Pacala, S.: Separating agricultural and non-agricultural fire seasonality at regional scales, Biogeosciences, 9, 3003–3012, doi:10.5194/bg-9-3003-2012, 2012.
Meehl, G. A. and Washington, W. M.: El Niño-like climate change in a model with increased atmospheric CO_2 concentrations, Nature, 382, 56–60, doi:10.1038/382056a0, 1996.
Mouillot, F. and Field, C. B.: Fire history and the global carbon budget: a $1^\circ \times 1^\circ$ fire history reconstruction for the 20th century, Glob. Change Biol., 11, 398–420, doi:10.1111/j.1365-2486.2005.00920.x, 2005.
Piao, S., Sitch, S., Ciais, P., Friedlingstein, P., Peylin, P., Wang, X., Ahlström, A., Anav, A., Canadell, J. G., Cong, N., Huntingford, C., Jung, M., Levis, S., Levy, P. E., Li, J., Lin, X., Lomas, M. R., Lu, M., Luo, Y., Ma, Y., Myneni, R. B., Poulter, B., Sun, Z., Wang, T.,

GMDD
7, 9017–9062, 2014

Viovy, N., Zaehle, S., and Zeng, N.: Evaluation of terrestrial carbon cycle models for their response to climate variability and to CO_2 trends, Glob. Change Biol., 19, 2117–2132, doi:10.1111/gcb.12187, 2013.

Podgorny, I. A., Li, F., and Ramanathan, V.: Large aerosol radiative forcing due to the 1997 Indonesian Forest Fire, Geophys. Res. Lett., 30, 1028, doi:10.1029/2002GL015979, 2003.

Prentice, I. C., Kelley, D. I., Foster, P. N., Friedlingstein, P., Harrison, S. P., and Bartlein, P. J.: Modeling fire and the terrestrial carbon balance, Global Biogeochem. Cy., 25, GB3005, doi:10.1029/2010GB003906, 2011.

Prudhomme, C., Giuntoli, I., Robinson, E. L., Clark, D. B., Arnell, N. W., Dankers, R., Fekete, B. M., Franssen, W., Gerten, D., Gosling, S. N., Hagemann, S., Hannah, D. M., Kim, H., Masaki, Y., Satoh, Y., Stacke, T., Wada, Y., and Wisser, D.: Hydrological droughts in the 21st century, hotspots and uncertainties from a global multimodel ensemble experiment, P. Natl. Acad. Sci. USA, 111, 3262–3267, doi:10.1073/pnas.1222473110, 2013.

Randerson, J. T., Chen, Y., van der Werf, G. R., Rogers, B. M., and Morton, D. C.: Global burned area and biomass burning emissions from small fires, J. Geohys. Res.-Biogeo., 117, G04012, doi:10.1029/2012JG002128, 2012.

Rocha, A. V. and Shaver, G. R.: Postfire energy exchange in arctic tundra: the importance and climatic implications of burn severity, Glob. Change Biol., 17, 2831–2841, doi:10.1111/j.1365-2486.2011.02441.x, 2011.

Rogers, A.: The use and misuse of V c, max in Earth System Models, Photosynth. Res., 119, 15–29, doi:10.1007/s11120-013-9818-1, 2014.

Ropelewski, C. F. and Halpert, M. S.: Global and regional scale precipitation patterns associated with the El Niño/Southern Oscillation, Mon. Weather Rev., 115, 1606–1626, doi:10.1175/1520-0493(1987)115<1606:GARSPP>2.0.CO;2, 1987.

Ropelewski, C. F. and Halpert, M. S.: Quantifying Southern Oscillation–Precipitation relationships, J. Climate, 9, 1043–1059, doi:10.1175/1520-0442(1996)009<1043:QSOPR>2.0.CO;2, 1996.

Roy, D. P., Boschetti, L., Justice, C. O., and Ju, J.: The collection 5 MODIS burned area product – global evaluation by comparison with the MODIS active fire product, Remote Sens. Environ., 112, 3690–3707, doi:10.1016/j.rse.2008.05.013, 2008.

Schimel, D. and Baker, D.: Carbon cycle: the wildfire factor, Nature, 420, 29–30, doi:10.1038/420029a, 2002.

GMDD
7, 9017–9062, 2014

Staver, A. C., Archibald, S., and Levin, S. A.: The global extent and determinants of savanna and forest as alternative biome states, Science, 334, 230–232, doi:10.1126/science.1210465, 2011.

Tansey, K., Grégoire, J.-M., Defourny, P., Leigh, R., Pekel, J.-F., van Bogaert, E., and Bartholomé, E.: A new, global, multi-annual (2000–2007) burnt area product at 1 km resolution, Geophys. Res. Lett., 35, L01401, doi:10.1029/2007GL031567, 2008.

Thonicke, K., Spessa, A., Prentice, I. C., Harrison, S. P., Dong, L., and Carmona-Moreno, C.: The influence of vegetation, fire spread and fire behaviour on biomass burning and trace gas emissions: results from a process-based model, Biogeosciences, 7, 1991–2011, doi:10.5194/bg-7-1991-2010, 2010.

Timmermann, A., Oberhuber, J., Bacher, A., Esch, M., Latif, M., and Roeckner, E.: Increased El Niño frequency in a climate model forced by future greenhouse warming, Nature, 398, 694–697, doi:10.1038/19505, 1999.

Tosca, M. G., Randerson, J. T., Zender, C. S., Flanner, M. G., and Rasch, P. J.: Do biomass burning aerosols intensify drought in equatorial Asia during El Niño?, Atmos. Chem. Phys., 10, 3515–3528, doi:10.5194/acp-10-3515-2010, 2010.

Turetsky, M. R., Kane, E. S., Harden, J. W., Ottmar, R. D., Manies, K. L., Hoy, E., and Kasischke, E. S.: Recent acceleration of biomass burning and carbon losses in Alaskan forests and peatlands, Nat. Geosci., 4, 27–31, doi:10.1038/ngeo1027, 2011.

Ward, D. S., Kloster, S., Mahowald, N. M., Rogers, B. M., Randerson, J. T., and Hess, P. G.: The changing radiative forcing of fires: global model estimates for past, present and future, Atmos. Chem. Phys., 12, 10857–10886, doi:10.5194/acp-12-10857-2012, 2012.

van der Werf, G. R., Randerson, J. T., Collatz, G. J., Giglio, L., Kasibhatla, P. S., Arellano, A. F., Olsen, S. C., and Kasischke, E. S.: Continental-scale partitioning of fire emissions during the 1997 to 2001 El Niño/La Niña Period, Science, 303, 73–76, doi:10.1126/science.1090753, 2004.

van der Werf, G. R., Randerson, J. T., Giglio, L., Collatz, G. J., Kasibhatla, P. S., and Arellano Jr., A. F.: Interannual variability in global biomass burning emissions from 1997 to 2004, Atmos. Chem. Phys., 6, 3423–3441, doi:10.5194/acp-6-3423-2006, 2006.

van der Werf, G. R., Dempewolf, J., Trigg, S. N., Randerson, J. T., Kasibhatla, P. S., Giglio, L., Murdiyarso, D., Peters, W., Morton, D. C., Collatz, G. J., Dolman, A. J., and DeFries, R. S.: Climate regulation of fire emissions and deforestation in equatorial Asia, P. Natl. Acad. Sci. USA, 105, 20350–20355, doi:10.1073/pnas.0803375105, 2008.

GMDD
7, 9017–9062, 2014

van der Werf, G. R., Morton, D. C., DeFries, R. S., Olivier, J. G. J., Kasibhatla, P. S., Jackson, R. B., Collatz, G. J., and Randerson, J. T.: CO_2 emissions from forest loss, Nat. Geosci., 2, 737–738, doi:10.1038/ngeo671, 2009.

van der Werf, G. R., Randerson, J. T., Giglio, L., Collatz, G. J., Mu, M., Kasibhatla, P. S., Morton, D. C., DeFries, R. S., Jin, Y., and van Leeuwen, T. T.: Global fire emissions and the contribution of deforestation, savanna, forest, agricultural, and peat fires (1997–2009), Atmos. Chem. Phys., 10, 11707–11735, doi:10.5194/acp-10-11707-2010, 2010.

van Leeuwen, T. T., van der Werf, G. R., Hoffmann, A. A., Detmers, R. G., Rücker, G., French, N. H. F., Archibald, S., Carvalho Jr., J. A., Cook, G. D., de Groot, W. J., Hély, C., Kasischke, E. S., Kloster, S., McCarty, J. L., Pettinari, M. L., Savadogo, P., Alvarado, E. C., Boschetti, L., Manuri, S., Meyer, C. P., Siegert, F., Trollope, L. A., and Trollope, W. S. W.: Biomass burning fuel consumption rates: a field measurement database, Biogeosciences Discuss., 11, 8115–8180, doi:10.5194/bgd-11-8115-2014, 2014.

Westerling, A. L., Turner, M. G., Smithwick, E. A. H., Romme, W. H., and Ryan, M. G.: Continued warming could transform Greater Yellowstone fire regimes by mid-21st century, P. Natl. Acad. Sci. USA, 108, 13165–13170, doi:10.1073/pnas.1110199108, 2011.

Wirth, C.: Fire regime and tree diversity in boreal forests: implications for the carbon cycle, in: Forest Diversity and Function, edited by: Scherer-Lorenzen, D. M., Körner, P. D. C., and Schulze, P. D. E.-D., Springer Berlin Heidelberg, 309–344, abailable at: http://link.springer.com/chapter/10.1007/3-540-26599-6_15 (last access: 17 November 2014), 2005.

Yue, C., Ciais, P., Cadule, P., Thonicke, K., Archibald, S., Poulter, B., Hao, W. M., Hantson, S., Mouillot, F., Friedlingstein, P., Maignan, F., and Viovy, N.: Modelling the role of fires in the terrestrial carbon balance by incorporating SPITFIRE into the global vegetation model ORCHIDEE – Part 1: simulating historical global burned area and fire regimes, Geosci. Model Dev., 7, 2747–2767, doi:10.5194/gmd-7-2747-2014, 2014.

Zhao, M. and Running, S. W.: Drought-induced reduction in global terrestrial net primary production from 2000 through 2009, Science, 329, 940–943, doi:10.1126/science.1192666, 2010.

GMDD
7, 9017–9062, 2014

Table 1. Comparison of simulated and GFED3.1 fire carbon emissions, burned area and total fuel consumption (TFC, including consumption of surface dead litter or organic soil, and live biomass) for different regions averaged over 1997–2009. The locations of the GEFD regions are mapped in Fig. S5, the abbreviations expanded in the caption to Fig. 4. The last three columns provide a qualitative indication of the error in simulated carbon emissions and its attribution to those of burned area and TFC.

Region	Emissions ($Tg\,C\,yr^{-1}$)		Burned area ($Mha\,yr^{-1}$)		Total fuel consumption ($g\,C\,m^{-2}$ of BA)		Emission error	BA error	TFC error
	GFED3.1	ORC	GFED3.1	ORC	GFED3.1	ORC			
BONA	54	45	2.1	3.3	2662	1385	=	=	−
TENA	9	96	1.5	18.5	627	514	+ + +	+ + +	=
CEAM	20	29	1.4	4.1	1489	714	=	+	−
NHSA	22	79	2.1	5.8	1007	1351	++	+	+
SHSA	272	369	20	35.7	1311	1035	=	+	=
EURO	4	13	0.7	1.5	667	874	++	+	+
MIDE	2	24	0.9	8.8	198	278	+ + +	+ + +	+
NHAF	480	680	129	58.7	377	1159	+	−	++
SHAF	556	331	125	34.1	448	969	−	−−	+
BOAS	128	61	6.6	3.9	1979	1589	−	−	=
SEAS	103	40	14	4.1	253	969	−	−	++
CEAS	35	161	7	41.4	1459	388	++	++	−−
EQAS	181	2	1.8	0.1	9500	1559	−−	−−	−−
AUST	133	174	52	15.6	259	1118	=	−	++

To obtain the qualitative error information, the ratio of simulated value to GFED3.1 is compared to the coefficient of variation (CV) of the corresponding GFED3.1 value as following:
=, no error, if the ratio is within (1 – CV, 1 + CV);
+, overestimated, if the ratio falls in (1 + CV, 3);
++, highly overestimated, if the ratio falls in (3,10);
+ + +, very much highly overestimated, if the ratio is bigger than 10;
−, underestimated, if the ratio falls in (0.3, 1 – CV);
−−, highly underestimated, if the ratio falls in (0.1, 0.3).
The CV for annual emissions and burned area by GFED3.1 data was calculated using the annual time series. Total fuel consumption data for GFED3.1 were obtained from Table 4 of van der Werf et al. (2010) and an arbitrary CV of 0.3 was adopted.

GMDD
7, 9017–9062, 2014

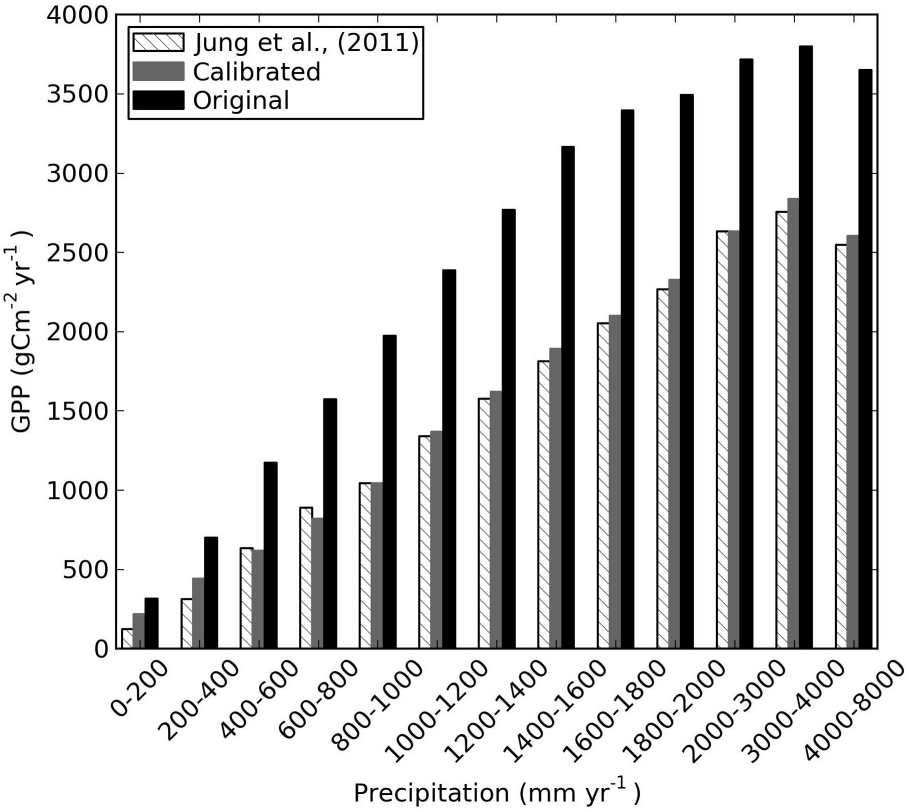

Figure 1. Annual GPP as a function of annual precipitation according to Jung et al. (2011) (dashed bar), model simulation before (black bar) and after calibration (grey bar).

GMDD
7, 9017–9062, 2014

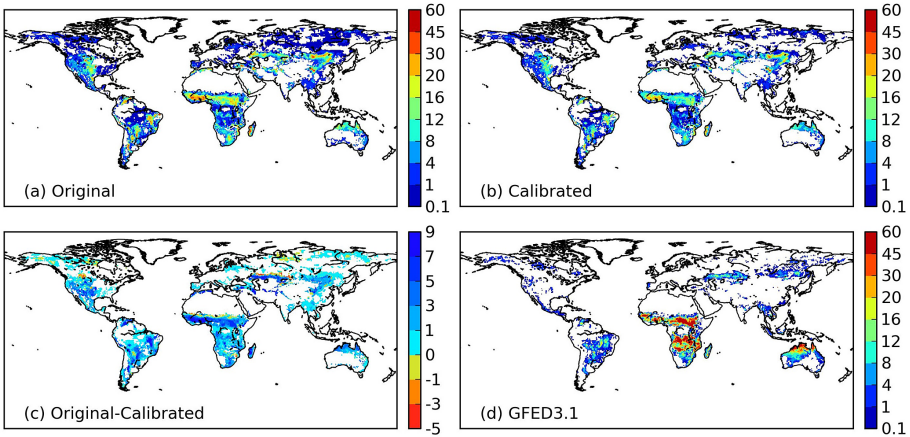

Figure 2. Simulated mean annual burned fraction (%) for 1997–2009 for **(a)** original and **(b)** calibrated model productivity. The change in burned fraction (original – calibrated) is shown in panel **(c)**, and the burned fraction by GFED3.1 data is shown in panel **(d)**.

GMDD
7, 9017–9062, 2014

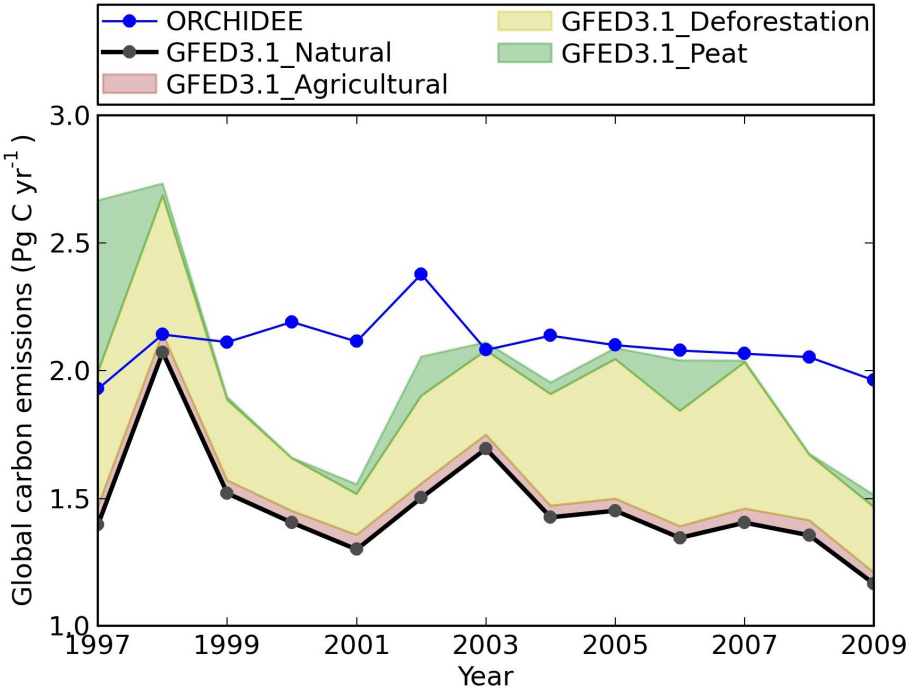

Figure 3. Annual global fire carbon emissions for 1997–2009 simulated by ORCHIDEE (blue), and from the GFED3.1 data. Carbon emissions from natural sources (forest fire, grassland fire, and woodland fire) are shown as the black solid line. Carbon emissions from agricultural fire, deforestation fire and peat fire (which are not explicitly simulated in ORCHIDEE) are shown as shaded areas stacked on top of GFED3.1 natural source fire carbon emissions.

GMDD
7, 9017–9062, 2014

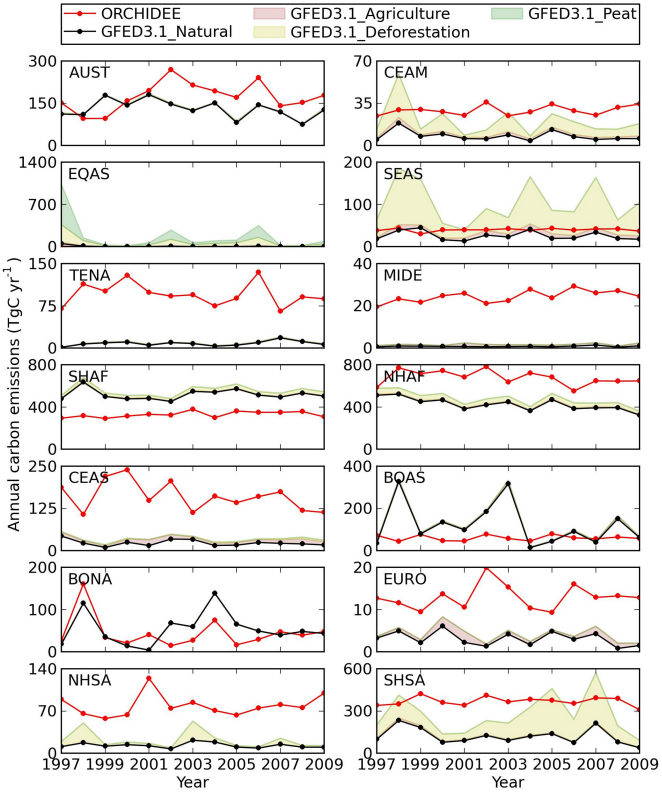

Figure 4. Annual fire carbon emissions simulated by ORCHIDEE and from the GFED3.1 data for 1997–2009 for the 14 different GFED regions. The 14 GFED regions are, BONA: Boreal North America; TENA: Temperate North America; CEAM: Central America; NHSA: Northern Hemisphere South America; SHSA: Southern Hemisphere South America; EURO: Europe; MIDE: Middle East; NHAF: Northern Hemisphere Africa; SHAF: Southern Hemisphere Africa; BOAS: Boreal Asia; CEAS: Central Asia; SEAS: Southeast Asia; EQAS: Equatorial Asia; AUST: Australia and New Zealand. Refer to Fig. S5 for their distribution.

GMDD
7, 9017–9062, 2014

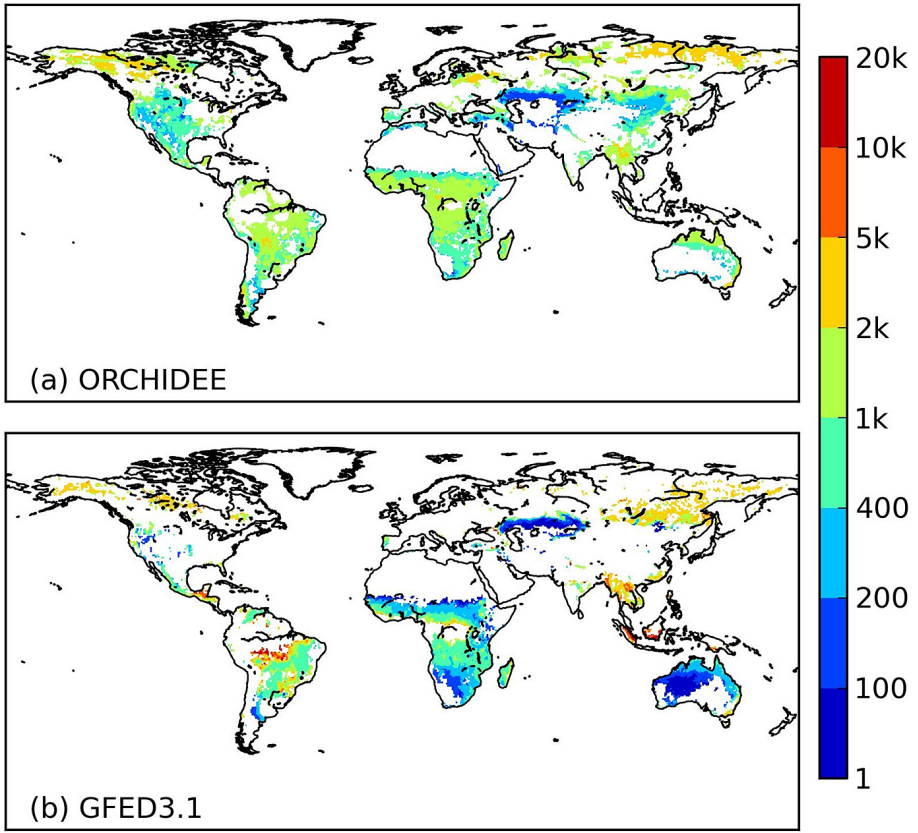

Figure 5. Fuel consumption ($g C m^{-2}$ of area burned) averaged over 1997–2009 by **(a)** ORCHIDEE simulation and **(b)** the GFED3.1 data.

GMDD
7, 9017–9062, 2014

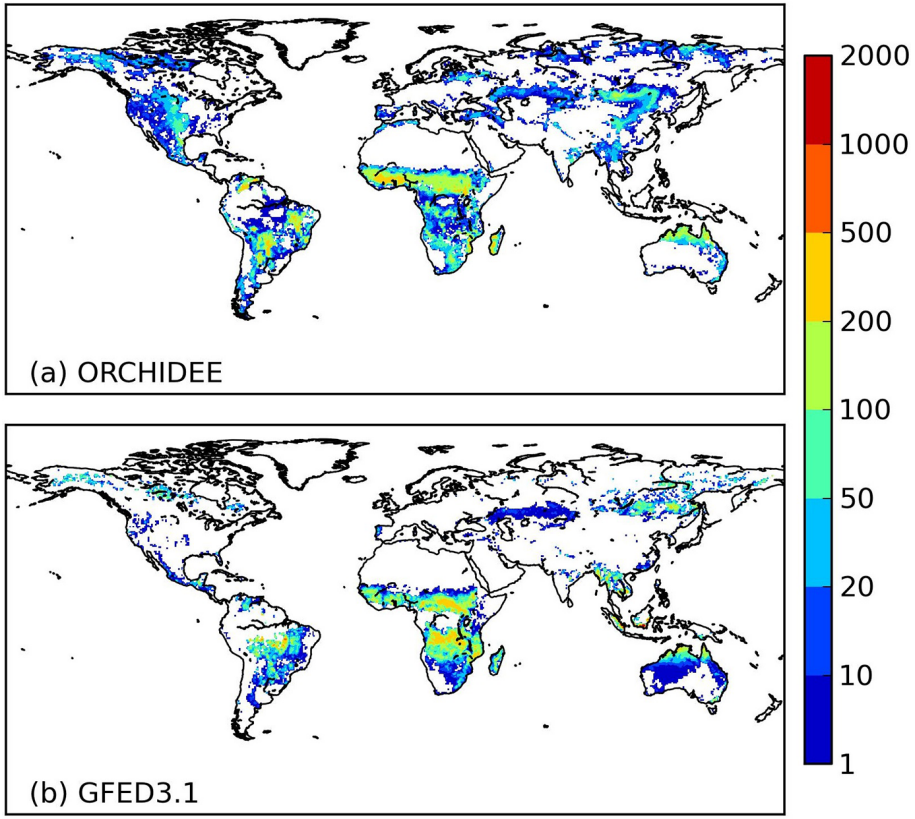

Figure 6. Mean annual carbon emissions ($g\,C\,m^{-2}\,yr^{-1}$) for 1997–2009 by **(a)** ORCHIDEE simulation and **(b)** the GFED3.1 data, based on the grid cell area.

GMDD
7, 9017–9062, 2014

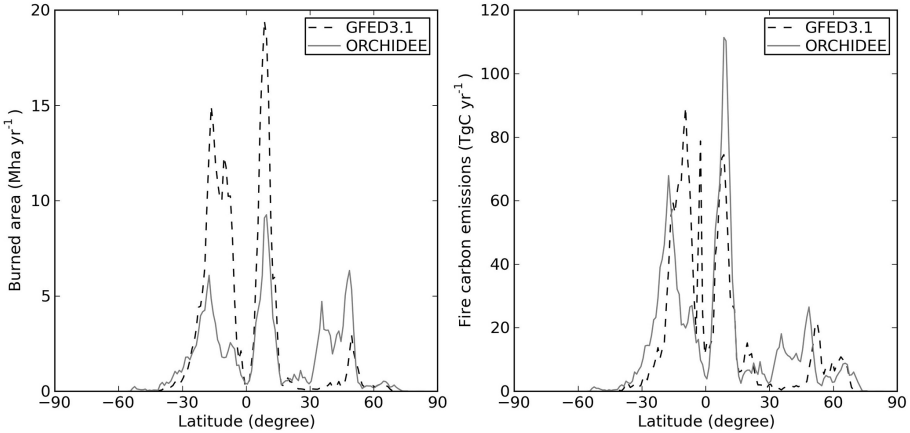

Figure 7. The latitudinal distribution of **(a)** burned area and **(b)** fire carbon emissions as simulated by ORCHIDEE (grey solid line) and by the GFED3.1 data (black dashed line).

GMDD
7, 9017–9062, 2014

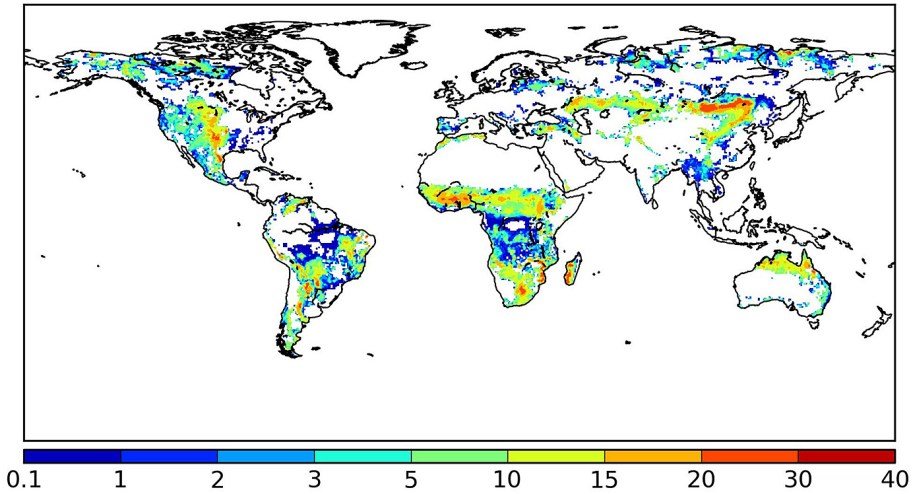

Figure 8. The fire carbon emissions returned to the atmosphere as percentage (%) of net primary production (NPP) for 2003–2012.

GMDD
7, 9017–9062, 2014

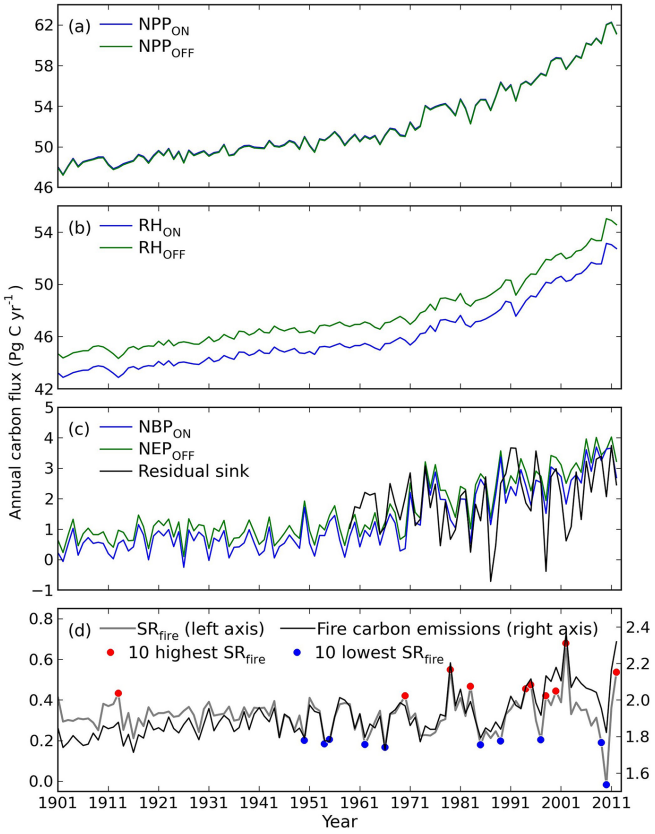

Figure 9. Different components of global carbon fluxes for fireON and fireOFF simulations. The carbon fluxes are **(a)** NPP; **(b)** heterotrophic respiration (RH); **(c)** NBP (NEP for fireOFF; NEP minus emissions for fireON) and the residual land sink as reported by Le Quéré et al. (2013); and **(d)** The NBP reduction by fires ($SR_{fire} = NBP_{OFF} - NEP_{ON}$, in grey, left vertical axis) and fire carbon emissions (black, right vertical axis).

GMDD
7, 9017–9062, 2014

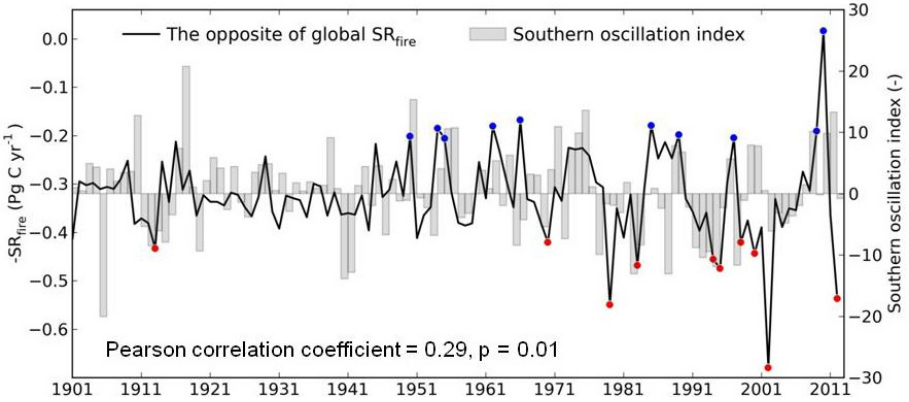

Figure 10. The fire-induced sink reduction (left vertical axis, $-SR_{fire}$) and its correlation with the Southern Oscillation Index (SOI, right vertical axis) which is an indicator for the El Niño Southern Oscillation (ENSO) climate oscillation. The red dots indicate the ten highest SR_{fire} years and the blue dots indicate the ten lowest SR_{fire} years. Note the left vertical axis shows the opposite of SR_{fire}.

GMDD
7, 9017–9062, 2014

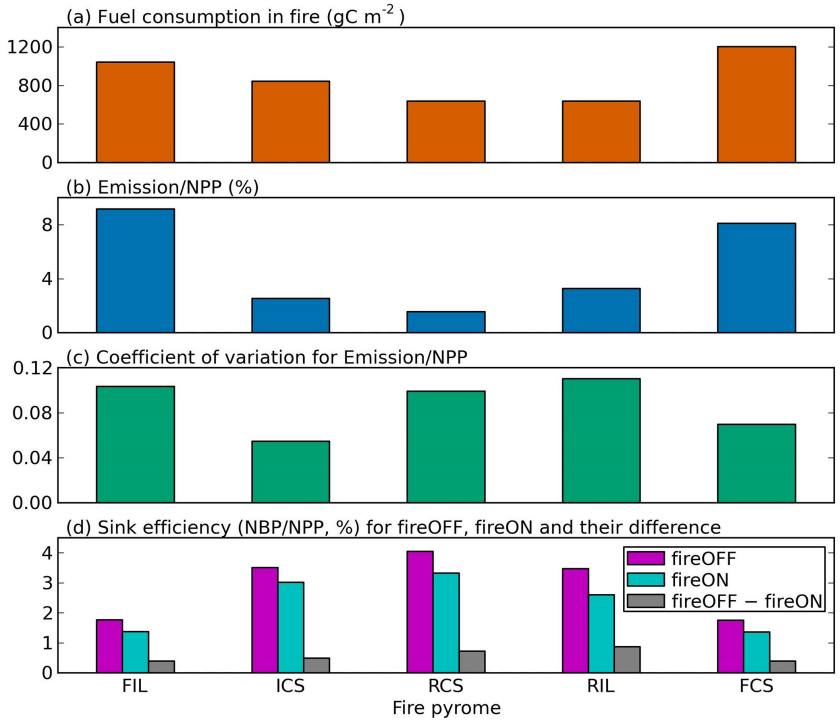

Figure 11. Characteristics of different fire pyromes (defined as by Archibald et al., 2013) in terms of the role of fires in the terrestrial carbon balance. **(a)** Fuel consumption in fire; **(b)** emissions as percentage of NPP; **(c)** coefficient of variation for the ratio of emission against NPP; and **(d)** sink efficiencies (for fireOFF, NEP_{OFF}/NPP_{OFF}; for fireON, NBP_{ON}/NPP_{ON}) for fireOFF and fireON simulations and their difference. All variables are shown for 1901–2012 except the fuel carbon consumption which is averaged over 2003–2012. The five fire pyromes are: FIL, Frequent–Intense–Large; ICS, Intermediate–Cool–Small; RCS, Rare–Cool–Small; RIL, Rare–Intense–Large; FCS, Frequent–Cool–Small. Refer to Fig. S2 for their spatial distribution.

GMDD
7, 9017–9062, 2014